Final Draft
of the original manuscript:

Brocks, W.; Scheider, I.; Schoedel, M.:
Simulation of crack extension in shell structures and prediction of residual strength
In: Archive of Applied Mechanics (2006) Springer

DOI: 10.1007/s00419-006-0041-9

Simulation of crack extension in shell structures and prediction of residual strength

Wolfgang Brocks, Ingo Scheider, Manfred Schödel

GKSS Research Centre, D-21402 Geesthacht

E-mail: brocks@gkss.de

Telephone: +49 4152 87 2553

Fax: +49 4152 87 2534

Abstract Two models for the numerical simulation of ductile crack extension in shell structures are presented and compared. They are based on the crack tip opening angle (CTOA) and a cohesive zone approach, respectively. After identification of the model parameters and investigations on the mesh dependence, the models are applied to various specimen configurations and structural components. Their excellent numerical performance favors their application for predicting the residual strength of lightweight components like aircraft fuselage.

Keywords crack extension, shell structures, residual strength, crack tip opening angle, cohesive model

1 Introduction

The certification of airplanes requires a series of complex and expensive test procedures on construction units of different kind, from specimens and single parts to the complete aircraft. Thus, the approval of new materials for use in aerospace industry as well as the implementation of optimized design represents an immense expense. Developing acknowledged methods for which some of these experiments can be replaced by numerical simulations is hence a big challenge [12].

Fracture mechanics has been established about 50 years ago as a means for describing crack initiation and extension in structures subject to monotonic or oscillatory loading. Specific quantities governing the singularities of stresses and strains at crack tips such as stress-intensity factor, K, or J-integral have been introduced as *crack-driving forces* in elasticity and elasto-plasticity, and analytical and numerical methods for calculating these quantities were developed, see overview in [2, 4]. On the other hand, test methods for measuring the material resistance to crack extension, so-called R-curves, have been implemented. Classical fracture mechanics, however, is mainly meant for heavy-section constructions such as pressure vessels, whereas lightweight structures make different demands on assessment methods. Standard J_R-curves are not adapted to describe crack extension in thin sheets and shells since the size requirements of the test standards are not met.

Present-day aircraft design is based on a damage tolerance concept [7, 9, 16], which acknowledges the existence of cracks and structural damage. The construction has to be designed in a way that any crack extension during service will not lead to catastrophic failure within the inspection intervals. The prediction of the residual strength of stiffened and un-stiffened thin-walled panels and shells in aircraft structures is an essential part of any damage tolerance analysis. Typical characteristics, which a respective failure assessment concept has to take into account, are

- Pronounced stable crack extension prior to failure and
- Constraint effects and related issues, which make any application of standard test methods for fracture toughness impossible or too conservative.

Analytical and numerical methods have been specifically adapted to thin-walled structures, for instance R-curve approaches based on the crack tip opening displacement (CTOD) [5, 19, 25, 30]. In the present paper, two models for the numerical simulation of ductile crack extension in shell structures are presented and compared. The first one is a node-release technique controlled by the crack-tip opening angle (CTOA) and the second one introduces particular interface elements allowing for material decohesion. All FE simulations have been executed under plane stress conditions, which required some modifications of the cohesive elements [6, 22].

2. Description of the Models

2.1 The Crack-Tip Opening Angle (CTOA)

In ductile materials, the crack tip blunts under increasing load until a critical value of the crack tip opening displacement (CTOD), δ, is reached and the crack starts extending. The subsequent crack extension can be characterized by an R-curve of δ in dependence on the crack extension, Δa, [19, 25]. After initiation no further crack-tip blunting occurs, and the deformation field is characterized by the crack tip opening angle (CTOA), ψ. This quantity is also suited for a criterion of crack extension,

$$\psi = \psi_{\mathrm{R}}(\Delta a)\,. \tag{1}$$

and the respective concept has been developed particularly for stable crack extension in thin sheets on the background of aerospace applications [17 - 19]. Crack extension is realized in the FE simulations by a *debond* or node release option controlled by the CTOA R-curve, eq. (1). The application of the CTOA criterion is for reasons of observability restricted to 2D (plane or shell) models, though a 3D application is presented in [13].

Within the validity limits of the CTOD concept, a geometrical relation exists between the CTOD R-curve, $\delta(\Delta a)$, and ψ,

$$\psi = \tan^{-1}\left(\frac{d\delta}{da}\right) \approx \frac{d\delta}{da}\,. \tag{2}$$

Despite numerous applications, there is still no unique definition for CTOA. A test standard for low constraint specimens [15, 26] is in process, however. The CTOA can be measured in-situ by optical microscopy and digital image correlation. The crack opening displacements are measured on the specimen surface over a certain distance behind the crack tip. A base length (BL) for measuring has to be defined in experimental tests as well as in numerical simulations, as this length will affect the results, see below in Fig. 5. Considering the resolution of optical measurements, it has been proposed in [14] to determine CTOA as the average value over a distance between 0.5 and 1.5mm behind the crack tip, that is a BL of 1 mm. Since the crack tip is frequently hard to detect, ψ is calculated from two pairs of points ahead of the crack tip connected by straight lines, see Fig. 1 (left). It can also be determined directly by post-mortem microtopography of the fracture surfaces [27, 29].

An indirect or inverse method of identifying CTOA is based on FE analyses of fracture mechanics tests. Crack extension is realized by a node release technique, in which the mesh has to consist of a regular arrangement of rectangular elements in the ligament, as shown in Fig. 1 (right). The CTOA R-curve, eq. (1), serves as the controlling parameter of crack extension. It is varied in repeated simulations in order to meet the experimental load-displacement record of the specimen.

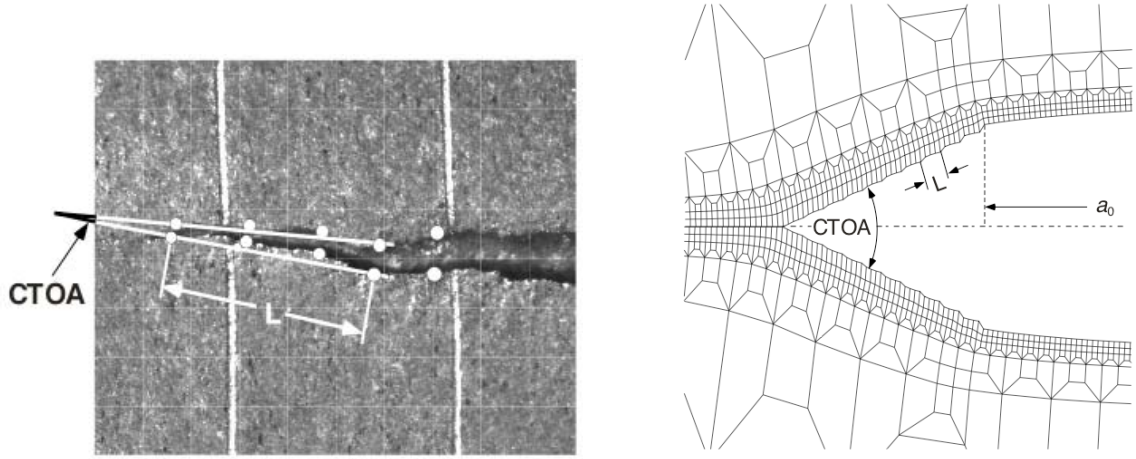

Figure 1: Experimental (left) and numerical (right) determination of the crack tip opening angle CTOA, L = base length

Measurements have shown that CTOA decreases after initiation and reaches a stationary value, ψ_c, after a transient phase [14]. Note, however, that these data may scatter significantly, see below in Fig. 3, which is a problem being particularly important for aerospace materials since the CTOA of aluminum alloys is in the order of only about 5 to 6°.

2.2 The Cohesive Model (CM)

Dugdale [11] and Barenblatt [1] introduced a cohesive zone ahead of the crack tip in order to avoid the unrealistic infinite stress at the crack tip, which is characteristic of the stress intensity factor approach. Modern phenomenological cohesive models (CM) describe various kinds of decohesion processes [3, 4] by a relation between surface tractions or cohesive stresses $\boldsymbol{\sigma}^{\mathrm{T}} = \{\sigma_{\mathrm{n}}, \sigma_{\mathrm{t}}, \sigma_{\mathrm{s}}\}$, having one normal and two tangential components and the material separation, $\boldsymbol{\delta}^{\mathrm{T}} = [\mathbf{u}]^{\mathrm{T}} = \{\delta_{\mathrm{n}}, \delta_{\mathrm{t}}, \delta_{\mathrm{s}}\}$. Cohesive surface elements are introduced at the boundaries

of solid elements along a pre-defined crack path. Various functions for the cohesive law, $\boldsymbol{\sigma} = \mathbf{f}(\boldsymbol{\delta})$, and numerous applications exist in the literature, see the overview given in [4]. Cohesive elements have in particular proven their ability in modeling crack extension in thin-walled panels [8, 20, 28].

The phenomenological constitutive relation of the interface elements, $\boldsymbol{\sigma} = \mathbf{f}(\boldsymbol{\delta})$, which cannot be measured directly, represents the effective mechanical behavior due to the physical processes of material separation or fracture. For ductile materials, the relevant separation mechanism is micro-void nucleation, growth and coalescence, and the cohesive parameters can get a micromechanical interpretation [3]. The various functions for the cohesive law used in the literature have in common, that they contain two characteristic parameters per crack opening mode, a cohesive strength, σ_c, and a critical separation, δ_c. Here, only mode I fracture is considered and a rather versatile cohesive law, $\sigma_n(\delta_n)$, is applied [21], which contains two additional shape parameters, δ_1 and δ_2,

$$\sigma_n(\delta_n) = \sigma_c \cdot \begin{cases} 2\left(\frac{\delta_n}{\delta_1}\right) - \left(\frac{\delta_n}{\delta_1}\right)^2 & \text{for } \delta_n \le \delta_1 \\ 1 & \text{for } \delta_1 < \delta_n \le \delta_2 \\ 2\left(\frac{\delta_n - \delta_2}{\delta_c - \delta_2}\right)^3 - 3\left(\frac{\delta_n - \delta_2}{\delta_c - \delta_2}\right)^2 + 1 & \text{for } \delta_2 \le \delta_n \le \delta_c \end{cases} , \qquad (3)$$

see Fig. 2. The interface elements are realized as user-defined element, UEL, in the FE code ABAQUS for 2D and 3D applications, and they were particularly adapted to plane stress and shell structures by incorporating the change of element thickness [6, 22].

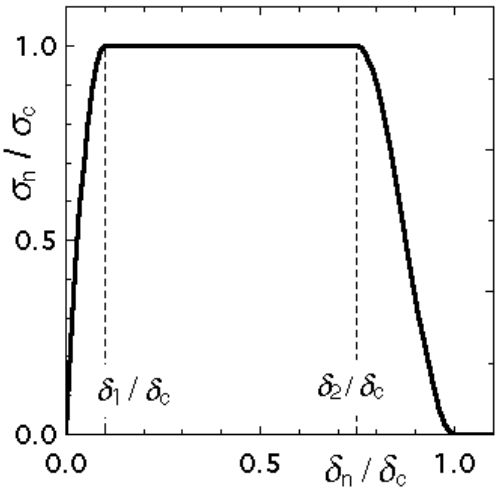

Figure 2: Cohesive law for $\delta_1 = 0.1\ \delta_c$, $\delta_2 = 0.75\ \delta_c$.

The parameter δ_1 in eq. (3) should be chosen as small as possible to obtain a high initial stiffness of the cohesive elements, as the deformation of the structure has to be dominated by the deformation of the solid elements. The parameter δ_2 allows for a variation between highly ductile, $\delta_2 \to \delta_1$, and quasi-brittle, $\delta_2 \to \delta_c$, fracture. Alternatively to δ_c, the separation energy, Γ_{Ic}, which simply represents the area under the traction-separation law,

$$\Gamma_{Ic} = \int_0^{\delta_c} \sigma_n(\delta_n)\, d\delta_n = \sigma_c \delta_c \left(\frac{1}{2} - \frac{1}{3}\frac{\delta_1}{\delta_c} + \frac{1}{2}\frac{\delta_2}{\delta_c} \right), \qquad (4)$$

can be introduced as a cohesive parameter. Estimates for the cohesive parameters in mode I fracture are the maximum true tensile stress at fracture of a notched tensile bar for the cohesive strength, σ_c, and the *J*-integral at crack initiation, J_i, for the separation energy, Γ_{Ic}, [3, 10]. A fine-tuning of the parameters by an FE simulation of a fracture mechanics test is recommended, however. Note, that the cohesive zone model is also applicable to the analysis of structures without cracks.

3 Model Verification

3. 1 Parameter Identification

The model parameters were determined for an aluminum alloy Al 5083 [23], which is used in shipbuilding and automotive industry. The thickness of the rolled panels is 3 mm. Various specimens have been manufactured from these panels, namely flat tensile specimens of 8 mm width for the determination of the stress-strain curve and fracture mechanics specimens of different sizes. The elastic properties are E = 70.3 GPa and ν = 0.33, and the proof stress is $R_{p0.2}$ = 242 MPa. Compact specimens, C(T), of widths W = 50 and 150 mm have been used to determine the parameters for CTOA and CM. As described above, direct measurements of the respective quantities were combined with FE simulations of fracture mechanics tests for a fine-tuning of the parameters.

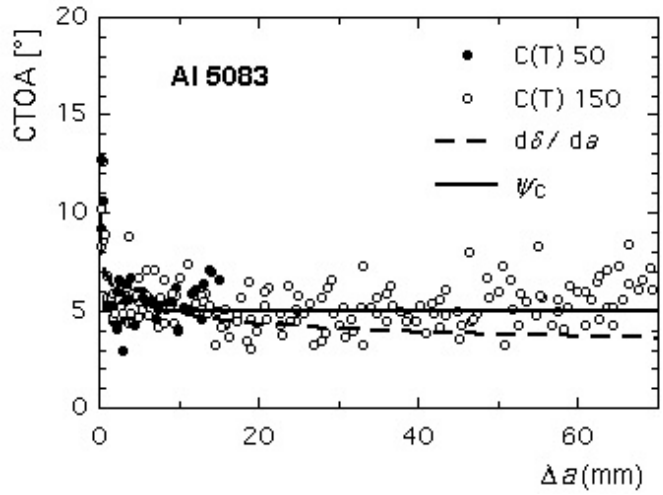

Figure 3: Optically determined CTOA values [14] with BL = 1 mm for Al 5083 from C(T) specimens of width W = 50, 150 mm and ψ_R-curve from parameter optimization.

The results of optical CTOA measurements for an aluminum alloy Al 5083 [14] are presented in Fig. 3. As also shown in the figure, the relation to the slope of the δ_R-curve holds until a crack extension of 15-20 mm. The transient part of the CTOA R-curve was hence taken from the derivative of an exponential fit of the δ_R-curve,

$$\delta_R = C\left(\frac{\Delta a}{\text{mm}}\right)^p + \delta_0 , \tag{5}$$

according to eq. (2), with C = 0.14 mm, p = 0.85, δ_0 = 0.17 mm. The definition of CTOD by Schwalbe [25] has been adopted here. Due to the scatter of the data, which exceeds any material specific differences, the stationary value, ψ_c, was determined by numerical simulations of the C(T) tests, see Fig. 4. The CTOA R-curve was finally identified as

$$\psi_R = \begin{cases} Cp\left(\dfrac{\Delta a}{\text{mm}}\right)^{p-1} & \text{for} \quad \Delta a < \Delta a_c \\ \psi_c & \text{for} \quad \Delta a \geq \Delta a_c \end{cases}, \tag{6}$$

with Δa_c = 8 mm, ψ_c = 5° [23].

The shape parameters of the cohesive law were chosen as $\delta_1 = 0.01\ \delta_c$ and $\delta_2 = 0.5\ \delta_c$, resulting in $\Gamma_{Ic} = 0.75\,\sigma_c\delta_c$. An estimate of the cohesive strength, σ_c, was obtained from the normal stress at fracture of the flat tensile specimen, and the separation energy, Γ_{Ic}, was pre-estimated from the J-integral at crack initiation measured in the C(T) tests. Subsequent optimization of the parameters by simulations of the load-displacement curve and the δ_R-curve of the C(T)50, see Fig. 4, yielded σ_c = 560 MPa and Γ_{Ic} = 10 kJ/m^2.

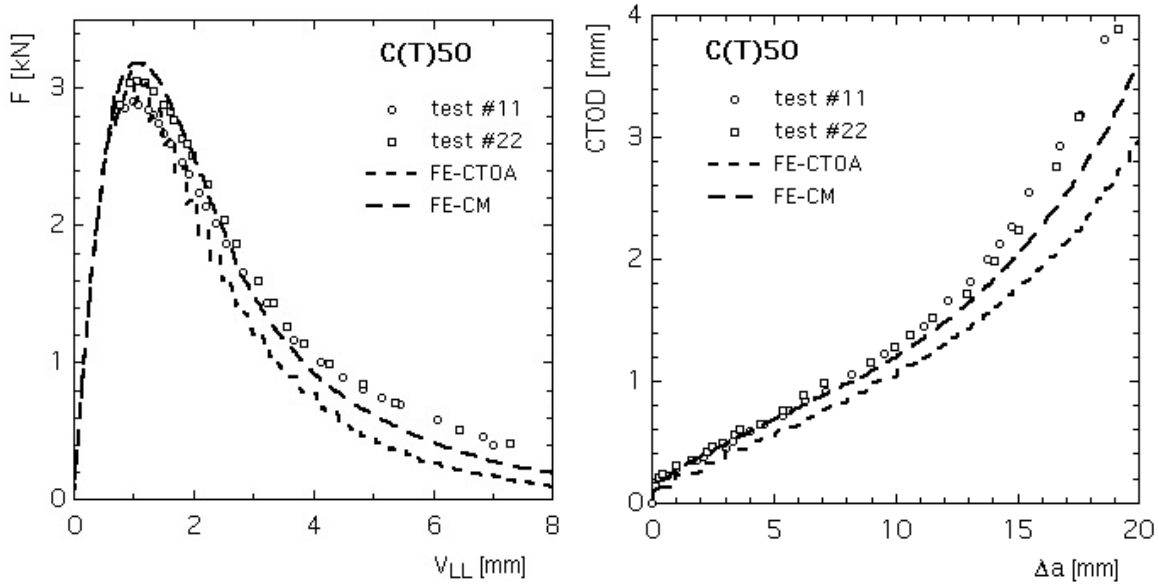

Figure 4: Parameter identification for CTOA and CM: experimental and simulated results of C(T) specimens, W = 50 mm, a_0/W = 0.5; load vs. load-line displacement curve (left) and δ_R-curve (right).

The transferability of all the model parameters to other specimen sizes and geometries like center-cracked panels, M(T), has been verified in [23].

3. 2 Mesh Dependence

Mesh dependence of numerical results is a big issue in damage mechanics, when softening behavior of materials is simulated. As the CTOA based simulations apply conventional

elasto-plastic constitutive equations, no pathological mesh dependence is expected, and the results are supposed to converge with decreasing element size. The base length for calculating CTOA affects the results, of course, as the crack edges are not straight near the crack tip. Both effects have been studied, and the relevant results are presented below.

Mesh-size dependence is also studied for the CM, which represents the softening and separation occurring in a material volume. As the cohesive law is expressed in terms of stresses in dependence on the separation, see eq. (3), a length scale parameter is inherent to the model [3]. Thus, no pathological mesh dependence is expected, either.

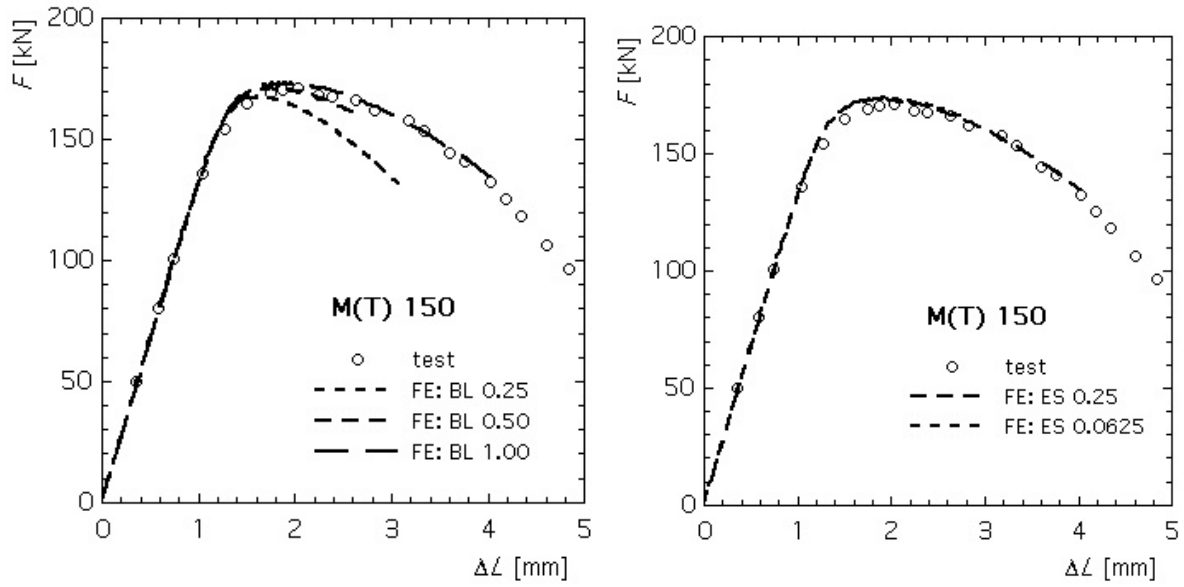

Figure 5: Simulation of crack extension in an M(T) specimen, $2W = 300$ mm, $a_0/W = 0.3$, by a CTOA R-curve: dependence on base length for ES = 0.25 mm, (left) and on element size for BL = 1.0 mm (right).

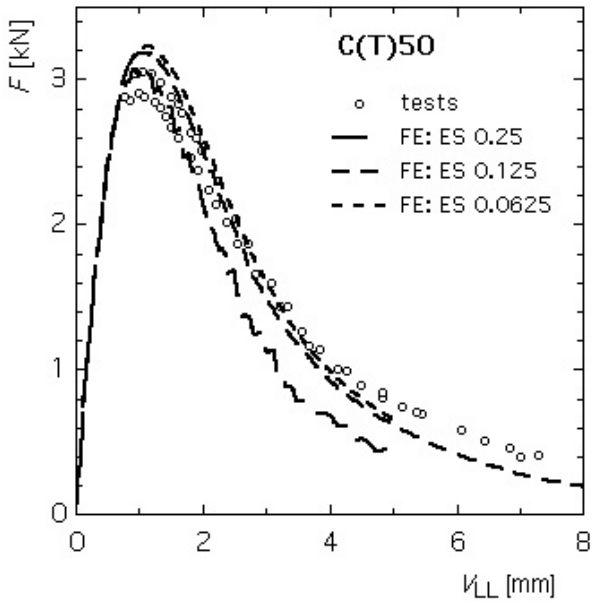

Figure 6: Simulation of crack extension by the CM in a C(T) specimen, $W = 50$ mm, $a_0/W = 0.5$: dependence on element size.

For investigating the effects of base length (BL) and element size (ES) on the simulation results for the CTOA based model, a center-cracked panel, M(T), of width $2W$ = 300 mm was chosen. A measuring length of L_0 = 1.5 W = 225 mm is used for the definition of elongation, ΔL. Taking the R-curve as determined above, the simulation with BL = 1.0 mm yields the correct response compared to the test data, see Fig 5 left, since the same BL was used in the optical evaluation of CTOA, Fig. 3. The effect of the element size (ES) for fixed BL is depicted in Fig. 5, right. Actually, no visible differences exist between the solutions for the two element sizes of 0.25 and 0.0625 mm.

Fig 6 finally demonstrates the effect of the element size for the CM which has been studied on a C(T) specimen as above. Here too, a decreasing ES for fixed BL yields a convergent solution. An element length of 0.125 mm was regarded as sufficient for the further calculations.

4. Application to Component-Like Structures

4. 1 Panel under Biaxial Tension

Real structural components are subject to biaxial loading. As a first validation step for the applicability of the models and the transferability of the model parameters to structures, crack growth in biaxially loaded cruciform panels of size $2W$ = 300 mm and relative initial crack length a_0/W = 0.2 has been investigated both experimentally and numerically [24], see Fig 7. Due to symmetry, the FE model is only one quarter of the specimen. The measuring length for elongation, ΔL, is $L_0 = 2W$ = 300 mm.

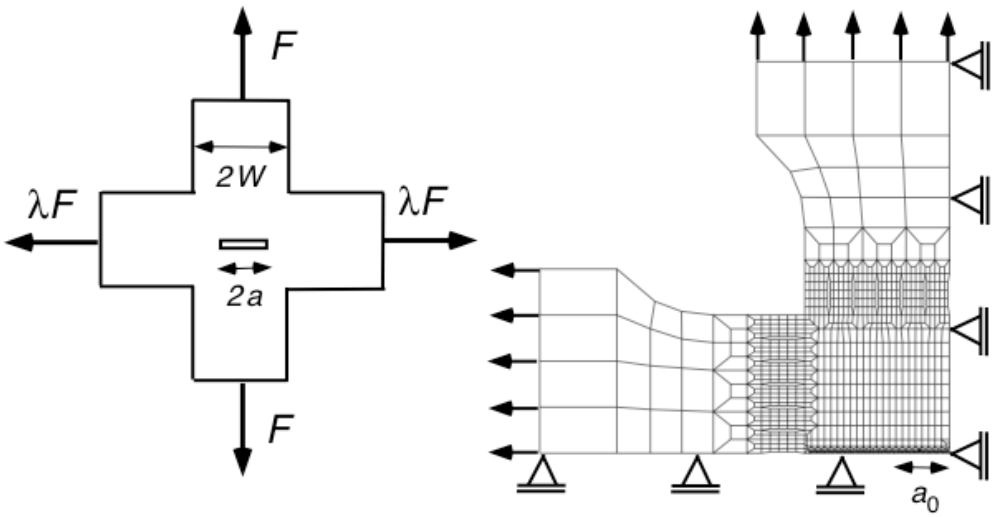

Figure 7: Biaxially loaded panel, schematic (left) and FE model (right).

The results of plane-stress FE simulations of crack extension in such a panel for a biaxiality ratio $\lambda = F_x/F_y = 0.5$ are compared to the test results in Fig. 8. Both models provide a fairly good prediction of the maximum load, i.e. the residual strength of the structure, though the respective δ_R-curves deviates significantly from those of the C(T) specimens for Δa > 8 mm, see Fig. 4. This confirms not only the transferability of the CTOA R-curve and of the

cohesive parameters from specimens to structures but clearly indicates, that a δ_R-curve would have failed in predicting the residual strength, as maximum load is reached for a crack extension of $\Delta a > 15$ mm.

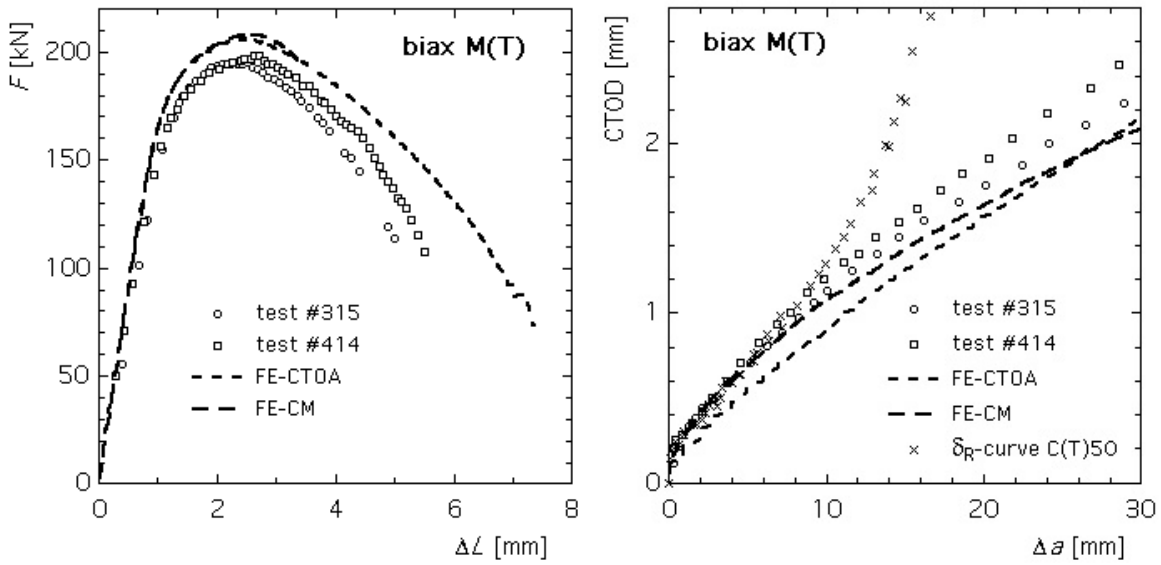

Figure 8: Biaxially loaded panel, biaxiality ratio $\lambda = 0.5$, load vs. elongation and δ_R-curve.

4. 2 Stiffened Cylinder

Cylindrical shells with circumferential stiffeners under internal pressure may be regarded as simplified models of an aircraft fuselage. The following examples, for which no experimental data are available, examine crack extension and residual strength of shells containing a crack located between two stringers, see Fig. 9. The FE model represents a 60° section of the total shell and accounts for symmetry.

As a debond option is not available for shell elements in ABAQUS, the respective CTOA-based simulations were executed with ANSYS utilizing the ANSYS Parametric Design Language (APDL). Fig. 10 depicts the pressure vs. crack-extension curves obtained by both models for an initial crack length of $2a_0 = 34$ mm. Due to the chosen base length for CTOA, the crack extension occurs in steps of 1 mm. The APDL implementation in ANSYS does not allow for a load decrease, so that the calculation stops at maximum load. The simulation with cohesive elements in ABAQUS permits a decreasing pressure by application of the Riks algorithm, and the crack extension occurs in steps of the element size, which is 0.125 mm, yielding a much smoother curve. The predicted values for maximum pressure are 0.97 and 0.90 MPa for the CTOA approach and the CM, respectively, which is a pretty fair accordance.

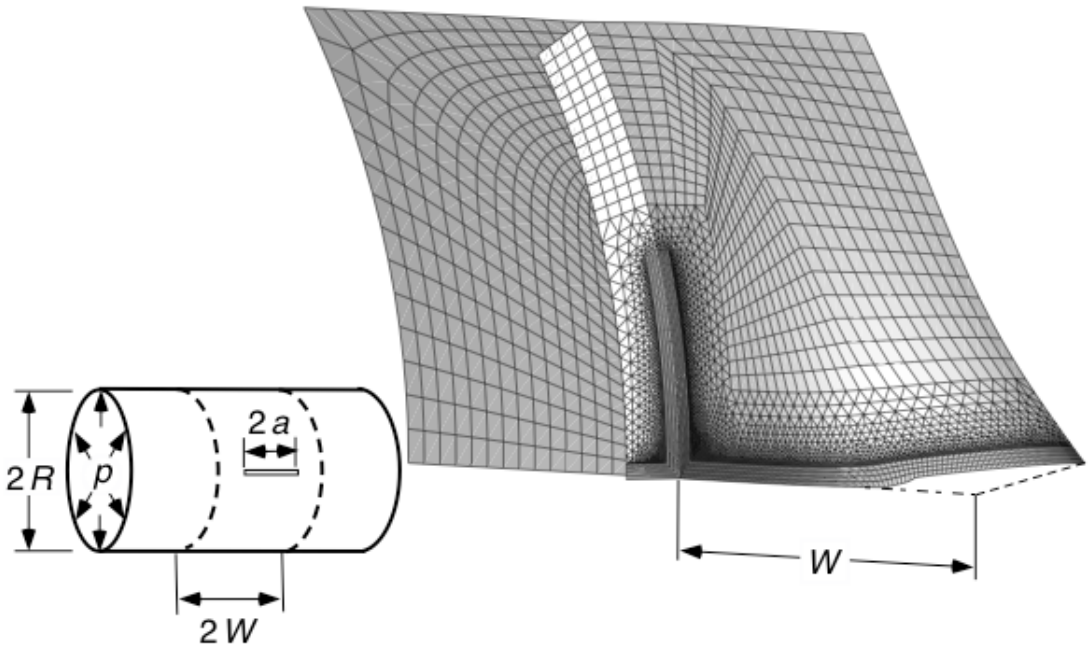

Figure 9: Stiffened cylinder with crack subject to internal pressure, diameter $2R$ = 100 mm, thickness of skin and stringer t = 1 mm, distance of stringers $2W$ = 100 mm; schematic of structure and deformed FE model.

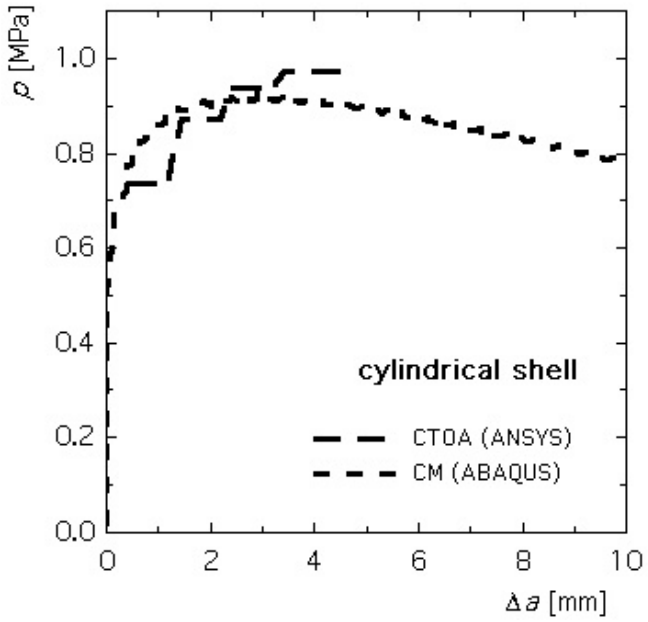

Figure 10: Stiffened cylinder with crack, pressure vs crack extension.

The CTOA model predicts the amount of crack extension but is not able to anticipate its orientation. The crack is assumed to extend in its original direction along the ligament. In the CM, the crack path is also restricted and predefined by the mesh, namely the arrangement of the cohesive elements. It offers a greater variability of the potential crack extension, nevertheless, as cohesive elements may be placed along various paths. In the second example of a pressurized cylindrical shell with a_0/W = 1.0, the location of cohesive elements allows for

crack extension in three directions, along a surface line of the skin, through the stringer and in circumferential direction along the stringer. Whereas the skin thickness was kept at 1 mm, the stringer thickness has been varied between 0.8 and 1.8 mm. The object of this parameter study was to find out: Does the crack extend keeping its original direction and thus rupture the stringer or does it deviate and extend in circumferential direction along the stringer without penetrating it.

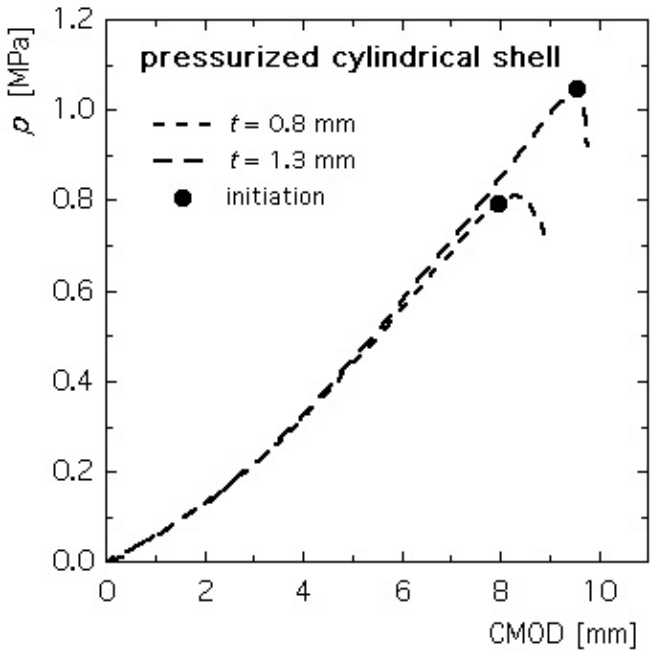

Figure 11: Pressure vs. crack opening displacement of cylindrical shell with two stringers containing a one-bay crack, effect of stringer thickness

The load-displacement curves for two stringer thicknesses, namely 1.3 and 1.8 mm, are shown in Fig 11. Maximum load is reached shortly after crack initiation. It increases remarkably, when the stringer thickness changes from 0.8 mm to 1.3 mm. No further increase was observed for t > 1.3 mm, however. The rising of maximum load corresponds to a change of the crack path. For a stringer thickness of 0.8 mm the crack extends in its original direction in the shell structure and through the stringer, see Fig. 13, left. For stringer thicknesses of 1.3 mm and 1.8 mm, the crack deviates at the stringer and extends circumferentially along the stringer without cutting it, see Fig. 13, right.

The effect of the stringer stiffness, which was studied here, may alternatively be regarded as an effect of the bonding strength of the stringer to the skin. In this case, the circumferential propagation of the crack would mean, that the stringer peels off, which can actually be observed in tests.

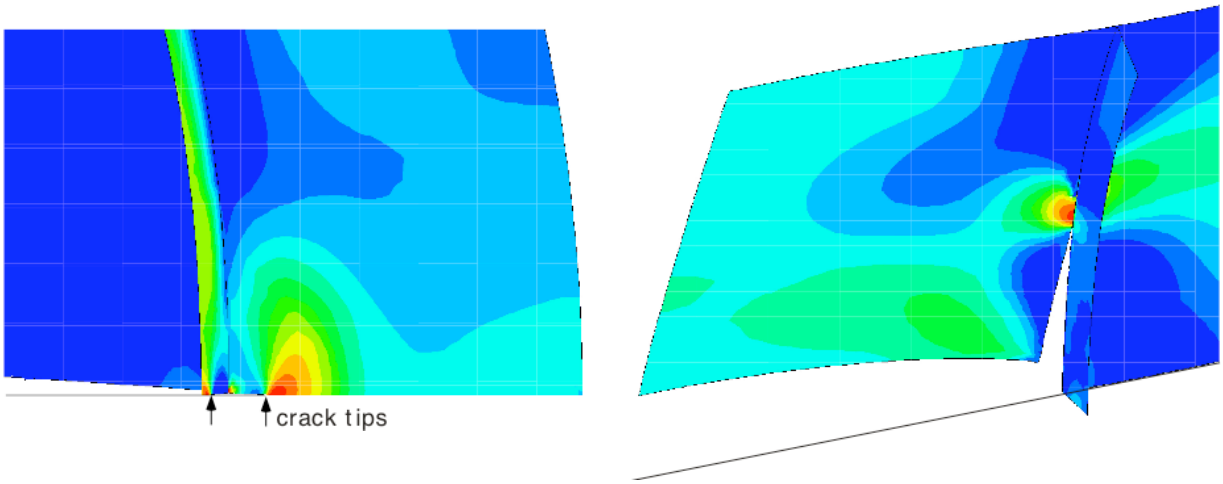

Figure 12: Crack extension in the pressurized cylindrical shell, effect of stringer thickness on crack path: (a) t = 0.8 mm, (b) t = 1.3 mm

Though no experimental data are available for validation, the broadly based experimental and numerical study of crack extension on C(T) and M(T) specimens in [23] documents the significance of the parameter studies performed on the shell structures.

5 Conclusions

The numerical simulations showed that large crack extensions in thin-walled panels can be predicted by a CTOA R-curve as well as by the cohesive model with good accuracy. The material parameters are physically motivated and can be rather easily determined from fracture tests on small C(T) specimens. They have proven to be transferable to larger structures and components. The excellent numerical performance of the two models favors their application for predicting the residual strength of components like aircraft fuselage. Whereas the CTOA criterion allows for a straightforward extension of the crack only, the cohesive elements can also predict possible crack-path deviations.

6 References

[1] Barenblatt, GI (1962) The mathematical theory of equilibrium cracks in brittle fracture. Adv Appl Mech 7: 55-129.

[2] Brocks, W (2004) Computational fracture mechanics. In: Raabe, D, Roters, F, Barlat, F, Chen, LQ (eds.): Continuum scale simulation of engineering materials. WILEY-VCH, Weinheim, pp. 621 - 637.

[3] Brocks, W (in press): Cohesive strength and separation energy as characteristic parameters of fracture toughness and their relation to micromechanics. Structural Integrity and Durability.

[4] Brocks, W, Cornec, A, Scheider, I. (2003): Computational aspects of nonlinear fracture mechanics. In: Milne, I, Ritchie, O, Karihaloo, B (eds.): Comprehensive structural integrity. Fracture of materials from nano to macro. Vol. 3, Elsevier, Oxford, pp. 127-209.

[5] Brocks, W, Nègre, P., Scheider, I., Schödel, M., Steglich, D., Zerbst, U. (2003): Structural integrity assessment by models of ductile crack extension in sheet metal. Steel Research 74, 504-13.

[6] Brocks, W, Scheider, I (in press): Cohesive elements for thin-walled structures. Comp Mat Sci.

[7] Broek, D. (1996): Concepts of fracture control and damage tolerance analysis. ASM International, Vol. 19, pp. 410-419.

[8] Chabanet, O, Steglich, D, Besson, J, Heitmann, V, Hellmann, D, Brocks, W (2003): Predicting crack growth resistance of aluminium sheets, Comp Mat Sci 26: 1-12.

[9] Congourdeau, F, Journet, B (2004): Damage tolerance of fuselage welded stiffened panels. ICAF 2003: 361-84.

[10] Cornec, A, Scheider, I, Schwalbe, KH (2003): On the practical application of the cohesive model. Engng Fracture Mech 70: 1963-87.

[11] Dugdale, DS (1960): Yielding of steel sheets containing slits. J Mech Phys Solids 8: 100-104.

[12] Fredriksson, B, Sjöström, L (1997): The role of mechanics and modelling in advanced product development. Eur J Mech A/Solids: 83-86.

[13] Gullerud, AS, Dodds, RH, Hampton, RW, Dawicke, DS (1999): 3-D modeling of ductile crack growth in thin metals: computational aspects and validation. Engng Fracture Mech 63: 347-374.

[14] Heerens, J, Schödel, M. (2003): On the determination of crack tip opening angle, CTOA, using light microscopy and δ_5 measurement technique. Engng Fracture Mech 70: 417-26

[15] ISO/TC 164/SC 4-N 413: Method of test for the determination of resistance to stable crack extension using specimens of low constraint. Draft Standard: Metallic Materials.

[16] Kaplan, MP, Wolff, TA (1996): Life extension and damage tolerance of aircraft. ASM International, Vol 19, pp. 557-565.

[17] Newman, JC (1999): Advances in fatigue and fracture mechanics analyses for aircraft structures. ICAF 2003: 3-42.

[18] Newman, JC, Bigelow, CA, Dawicke, DS (1999): Finite-element analyses and fracture simulation in thin-sheet aluminum alloy, Durability of Metal Aircraft Structures, Proc. Int. Workshop on Structural Integrity of Aging Airplanes, 1999, p. 167.

[19] Newman, JC, James, MA, Zerbst, U (2003): A review of the CTOA/CTOD fracture criterion. Engng Fracture Mech 70: 371-85.

[20] Roy, YA, Dodds, RH (2001): Simulation of ductile crack growth in aluminium panels using 3-D surface cohesive elements. Int J Fract 110: 21-45.

[21] Scheider, I (2000): Simulation of cup-cone fracture in round bars using the cohesive zone model. Proc. 1st MIT Conf. Computational Fluid and Solid Mechanics, pp. 460-462.

[22] Scheider, I, Brocks, W (2005): Simulation of crack propagation and failure in shell structures using the cohesive model. In: Ramm, E, Wall, WA, Bletzinger, KU, Bischoff, M (eds.): Proc 5th Int. Conf. Computation of Shell and Spatial Structures. Salzburg (A).

[23] Scheider, I, Schödel, M, Brocks, W, Schönfeld, W (2006): Crack propagation analyses with CTOA and cohesive model: Comparison and experimental validation, Engng Fracture Mech 73: 252-263.

[24] Scheider, I, Schödel, M, Schönfeld, W, Brocks, W (2005): Modelling crack extension in biaxially loaded panels. In: 11th Int Conf on Fracture, ICF 11, Turin (I). 5662.

[25] Schwalbe, KH (1995): Introduction of δ_5 as an operational definition of the CTOD and its practical use. ASTM STP 1256: 763-78.

[26] Schwalbe, KH, Newman, JC, Shannon; JL (2005): Fracture mechanics testing on specimens with low constraint – standardisation activities within ISO and ASTM. Engng. Fracture Mech 72: 557-76.

[27] Shan, GX, Kolednik, O, Fischer, FD, Stüwe, HP (1993): A 2D-model for the numerical investigations of the stable crack growth in thick smooth fracture mechanics specimens. Engng Fracture Mech 45: 99-106.

[28] Siegmund, T, Brocks, W (2000): Simulation of ductile crack growth in thin aluminum alloys. In: Halford, GR Gallagher, JP (eds.) 31st Nat Symp Fatigue and Fracture Mechanics, Cleveland (OH, USA), ASTM STP 1389, pp. 475 - 485.

[29] Stampfl, J, Scherer, S, Berchthaler, M, Gruber, M, Kolednik, O (1996): Determination of the fracture toughness by automatic image processing, Int J Fracture 78: 35-44.

[30] Zerbst, U, Brocks, W, Heerens, J, Schödel, M, Scheider, I, Steglich, D, Seib, E, Cornec, A, Schwalbe, KH (2005): Failure assessment concepts for thin-walled structures. In: Structural Integrity of Advanced Aircraft and Life Extension for Current Fleets, ICAF 2005. Hamburg (D).